

TIME DEPENDENT ANALYSIS OF A RECTANGULAR SYNTHETIC JET

Young-Hwan Kim*, Kevin P Garry**

*Emirates Aviation College, UAE, **Cranfield University, UK

yhkim@emirates.com; k.p.garry@cranfield.ac.uk

Keywords: Synthetic jet, Piezoelectric, Hotwire, Power spectra, Velocity profile

Abstract

A synthetic jet is a high frequency unsteady flow created as a result of cyclic suction and blowing through an orifice. A time averaged analysis of the flow structure within a synthetic jet is of limited value. In view of this, time dependent local velocity measurements, using a hot wire anemometer, are reported for a synthetic jet with a rectangular orifice of aspect ratio 70. Detailed measurements of local flow velocity, in quiescent conditions, within a control volume in the jet production region above the orifice exit plane, are presented. These data are analysed synchronous with the synthetic jet excitation signal to aid understanding of the periodic nature of resulting jet structure. Instantaneous velocity profiles, normalized velocity time histories and, normalized power spectra are used to understand the flow development and cyclic characteristics. Emphasis is placed on the jet development between the orifice exit plane and the point at which it becomes a steady jet at nominally 20 slot widths above the orifice.

1 Introduction

A Synthetic Jet can be created by the cyclic volume change of an internal cavity, which is connected to surrounding air through an orifice. There are many devices which can create a high frequency internal volume change and the piezoelectric diaphragm is selected as a bi-directional pumping device for the Synthetic Jet Generator (SJG) used in this study. An experimental investigation of the induced flow field is carried out, in quiescent conditions to simplify the assessment, as a precursor to the

possible utilization of such a device in low speed flow control applications.

2. Design of Piezoelectric-driven Synthetic Jet Generator

A piezoelectric diaphragm is a thin metal plate to which a piezoelectric ceramic is adhered to one face. Piezoelectric ceramic is a unique material which expands and contracts its planar area with the change of polarity of an applied electric field. Since the metal plate does not change its planar area, a high frequency alternating voltage will cause the piezoelectric diaphragm to vibrate as a result of the difference of deformation ratio between the two materials, see Figure 1.

A piezoelectric diaphragm supplied by *Murata Manufacturing Company* (product reference 7BB-50M-1) is used to fabricate the SJG used in this study. This particular diaphragm is designed for use in acoustic devices; it consists of a 50mm diameter nickel-plated brass disc with a 25mm diameter piezoelectric ceramic film on one face.

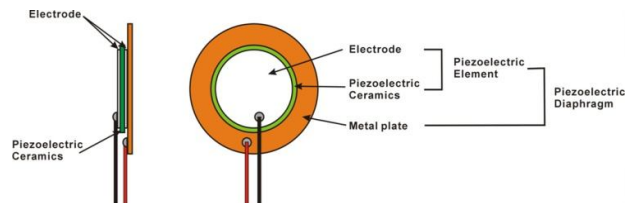


Fig. 1. Structure of a Piezoelectric Diaphragm, adapted from [10]

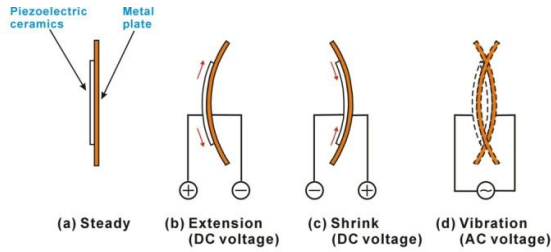


Fig. 2. Schematic illustration of the vibration mechanism of a Piezoelectric Diaphragm, adapted from [10]

The primary limitation of a piezoelectric diaphragm is its limited displacement and consequently the small internal volume change of the cavity to which it is connected. In view of this a SJG, which utilizes a dual diaphragm, was designed for the current study. Two piezoelectric diaphragms, arranged face-to-face, form the walls of the internal cavity, each driven by an identical excitation signal with a 180° phase difference, so as to maximise the volumetric change of the cavity. A schematic illustration of the mode of operation of the SJG is given in Figure 3. An expanded view of the various SJG components is given in Figure 4. The detailed design of this SJG is based on a study by Chambers et al [3]; in this case the rectangular slot is 35mm (long, L) × 0.5mm (wide, H). Note that the slot depth varies from 11 to 2.5mm, see Figure 6.

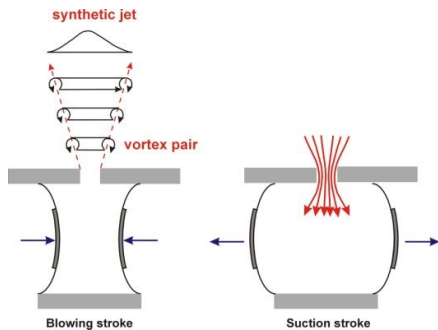


Fig. 3. Schematic illustration of the dual diaphragm SJG flow mechanism

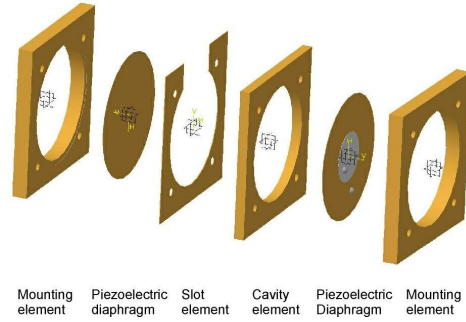


Fig. 4. Expanded view of key SJG components

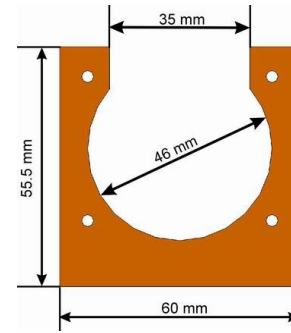


Fig. 5. Cross section of the cavity and slot element of the SJG

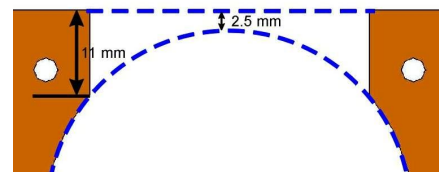


Fig. 6. Cross section of SJG cavity illustrating non-uniform slot depth

3 Experimental Arrangement

A schematic of the SJG excitation system and synthetic jet measurement arrangement is given in Figure 7. The output of a Dantec 55P11 single component hot wire anemometer (HWA) probe, mounted on a manual traversing system, is filtered and recorded digitally. A function generator creates an excitation signal at a frequency of 1500Hz. corresponding to the cavity resonance frequency of the SJG. The datum of the probe coordinate system is taken to be the centre of the slot and distances are non-dimensionalised using the slot width ($H=0.5\text{mm}$), see Figure 8. The sampling frequency(F_s) and low pass filter(LPF) are kept constant at 25 kHz, and 10 kHz, respectively.

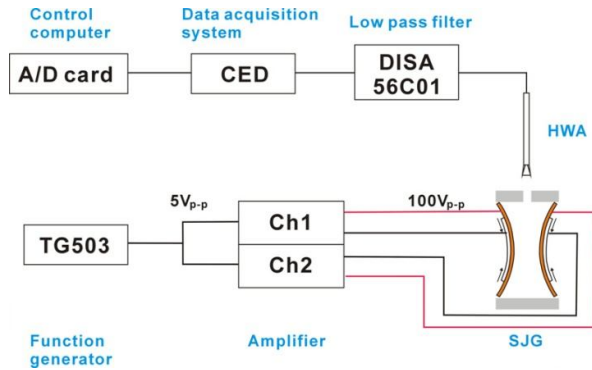


Fig. 7. Schematic arrangement of data acquisition and SJG excitation systems

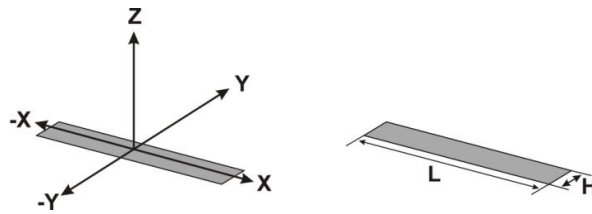


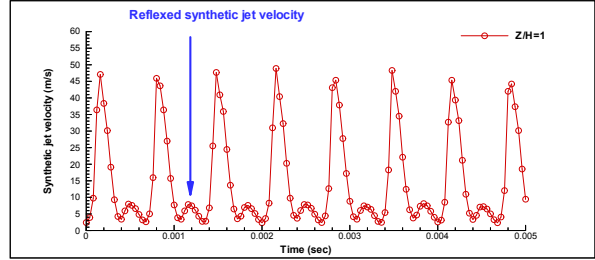
Fig. 8. Coordinate system adopted for HWA probe positioning, shown relative to the SJG slot exit plane (shaded)

4 Presentation and Discussion of Results

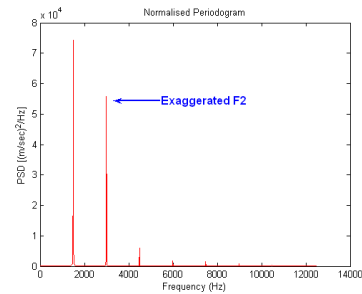
4.1 Optimum vertical range of HWA probe position.

A conventional HWA probe is unable to measure reversing flows (the so-called forward-reverse ambiguity) [7]. Whilst it is assumed that the key features of a synthetic jet will be predominately in close proximity to the slot exit plane, care must be taken to avoid positioning the HWA probe so close that it infringes the reverse flow ambiguity region. The reverse flow of synthetic jet (suction) results in a ‘mirror image’ in the synthetic jet velocity time history around the minimum measurable velocity [7]. The time history for the synthetic jet velocity shown in Figure 9(a) is typical of that seen in the reverse flow region and results in an exaggeration of the second harmonic (F2) in the corresponding power spectra, see Figure 9(b). This characteristic in the synthetic jet velocity

time history is not detected for probe positions where $Z/H \geq 3$ and therefore $Z/H = 3$ is taken as the ‘standard’ vertical position of the HWA probe in this study, see Figure 10.

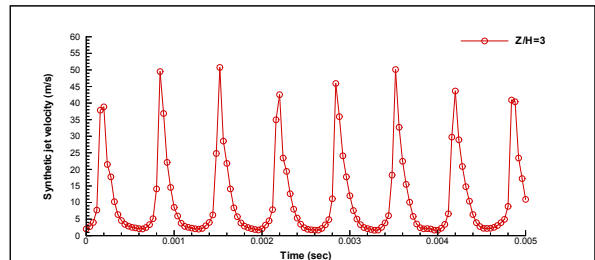


(a) Synthetic jet velocity time signature at X=Y=0

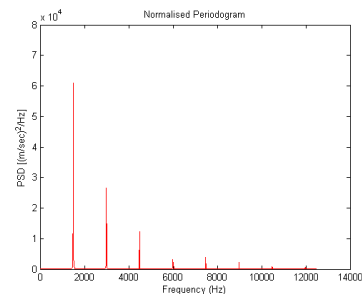


(b) Local velocity power spectra at X=Y=0

Fig. 9. HWA Analysis at $Z/H=1$ ($Z=0.5\text{mm}$)



(a) Synthetic jet velocity time signature at X=Y=0



(a) Local velocity power spectra at X=Y=0

Fig. 10. HWA analysis at $Z/H = 3$ ($Z=1.5\text{mm}$)

4.2 System frequency characteristics

Figure 11 presents the time history of two signals, recorded simultaneously, for five cycles of the SJG operation (at probe position: $X/H=0$, $Y/H=0$, $Z/H=3$). The square wave is the non-dimensionalised excitation signal, within which the end of each abrupt drop is taken to be the end of a cycle. The corresponding synthetic jet velocity time history is not exactly repeatable and therefore the average fluctuation of the synthetic jet velocity in a single cycle is calculated using an ensemble average. This averaged fluctuation is termed as a normalized time history (NTH) throughout this study.

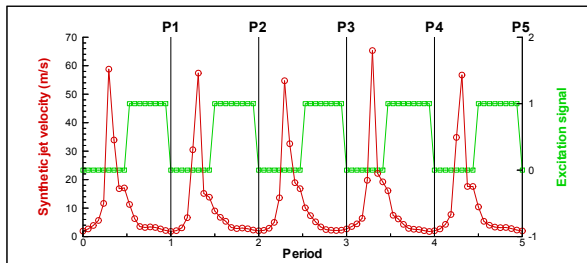


Fig. 11. Periodic Nature of Synthetic Jet Time History ($X/H=0$, $Y/H=0$, $Z/H=3$)

Figure 12 shows two possible operation modes of a dual diaphragm SJG; bi-directional and uni-directional vibration, the latter is used throughout this study. Previous work by Yao et al [5] and Schaeffler et al [6] show that there is time delay between the excitation signal, diaphragm displacement and a pressure change in the internal cavity. It is expected that there will be a similar delay between the resonance cavity pressure change and the formation of the synthetic jet. The velocity peaks in Figure 11 are seen to appear before the excitation signal discontinuity, which is responsible for the shrinking of the resonance cavity, in each cycle. These velocity peaks are possibly associated with flow initiated by the previous cycle, due to the time delay between the excitation signal and synthetic jet formation.

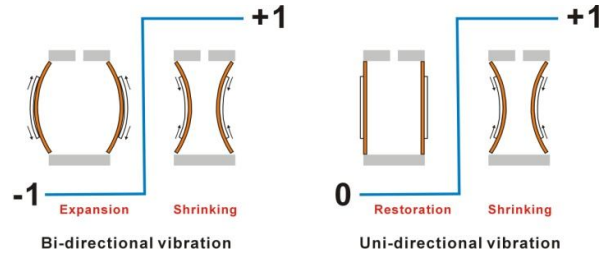
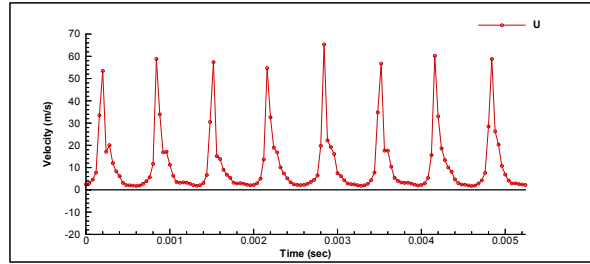
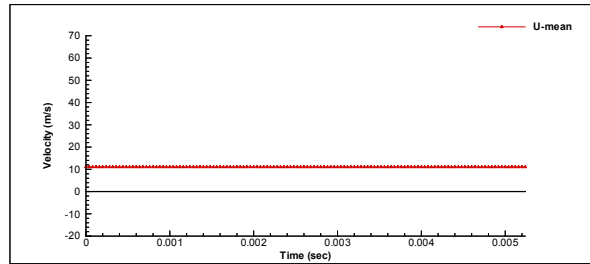


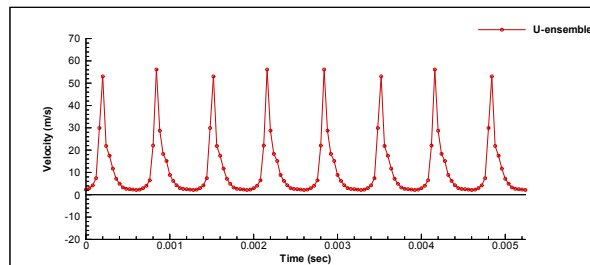
Fig. 12. Illustration of the cavity volume change due to piezoelectric diaphragm vibration for each of the excitation signal modes



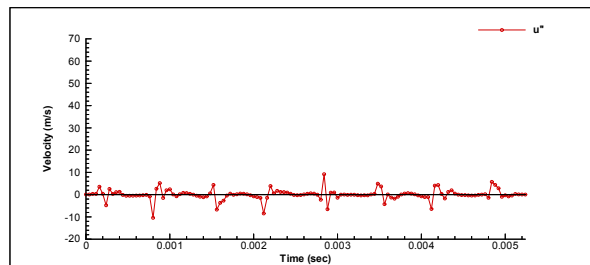
(a) Synthetic jet velocity time history (U)



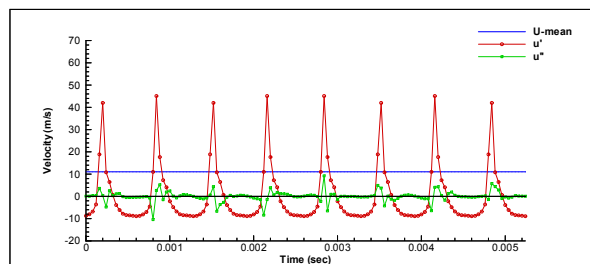
(b) Time averaged velocity (\bar{U})



(c) Ensemble averaged velocity ($\tilde{U} = \bar{U} + u'$)



(d) Velocity fluctuation around \tilde{U} (u'')



(e) Three velocity components of synthetic jet (\tilde{U} , u' , u'')

Fig. 13. Decomposition of a synthetic jet velocity time history ($X/H=0$, $Y/H=0$, $Z/H=3$, $F1=1.5\text{KHz}$)

4.3 Normalized time history analysis

Figures 14, 15 and 16 represents the change of local velocity NTH with position relative to the SJG slot datum. With a variation in longitudinal position(X), the peak velocity - which is created by the blowing stroke of the synthetic jet - appears at a phase angle of nominally 108° . The magnitude of the peak velocity is reduced and its phase angle is increased with increasing longitudinal distance from the slot centre (X/H). This means the jet momentum, which is created by the diaphragm vibration, is not uniformly distributed along the slot. The time delay and lower peak velocity in the vicinity of slot boundary is assumed to be caused by boundary layer development on the internal wall of the slot, see Figure 14. The variation of local velocity NTH in the transverse direction exhibits a secondary velocity peak at $Y/H > 0.8$. Since this induced flow has a (nominally) 162° phase difference from the peak velocity (blowing), it is assumed to be caused by the suction phase, which will have a 180° phase difference, see Figure 15.

The variation of local velocity NTH with vertical position shows that the nature of the synthetic jet is transformed from an unsteady jet to a steady jet as the HWA probe moves away from the slot exit plane. The degree of unsteadiness in the synthetic jet local velocity reduces with increasing vertical distance from the slot exit until $Z/H > 20$ when the synthetic jet becomes a steady jet, see Figure 16.

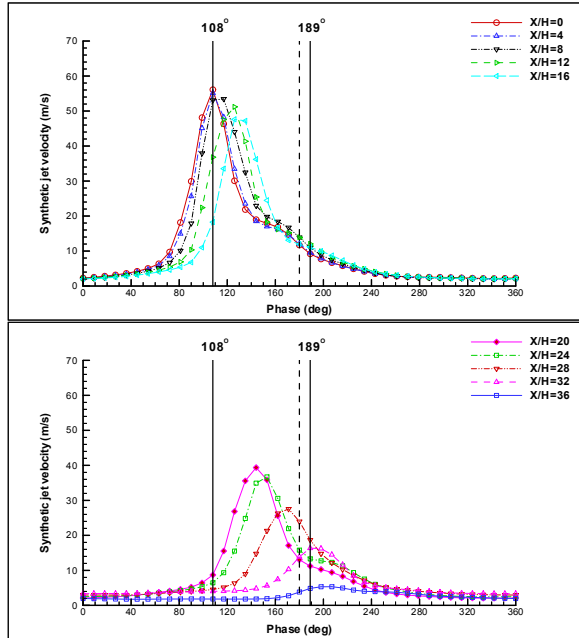


Fig. 14. Variation of local velocity NTH with position along the length of the slot (X/H)

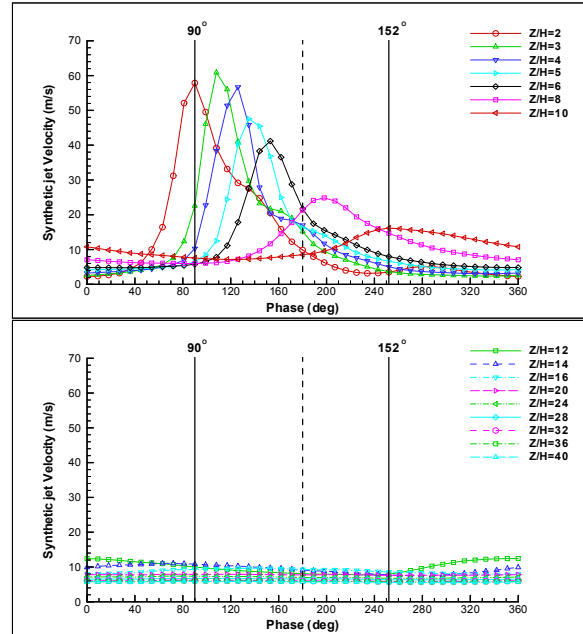


Fig. 16. Variation of local velocity NTH with position above the centre of the slot (Z/H)

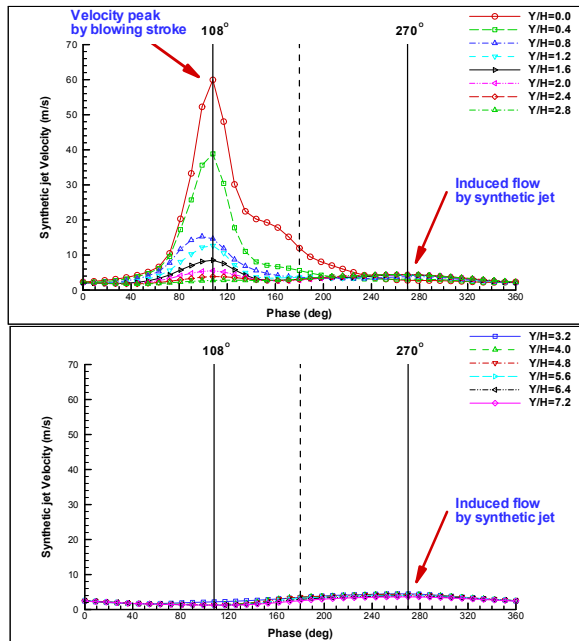


Fig. 15. Variation of local velocity NTH with position across the width of the slot (Y/H)

4.4 Change of peak velocity phase.

Figures 14 - 16 show that the phase of the peak local velocity in the jet is not consistent with location in each axis and these changes in phase are presented in Figures 17, 18 and 19, (the vertical dashed lines in Figure 17 and 18 represent the edge of the slot. The vertical solid lines in Figure 18 represent the border between the induced flow region and the synthetic jet region. The horizontal dashed line in Figure 19 represents the boundary between the unsteady jet region and the steady jet region). The change of peak velocity phase with longitudinal position corresponds to the time delay due to the momentum transfer from the diaphragm to the air, see Figure 17. The phase change in the transverse direction exhibits an abrupt change that is caused by the formation of induced flow from the surrounding air, which is assumed to be caused by the suction phase of synthetic jet. Figure 19 shows that the peak velocity phase of the synthetic jet increases with increasing distance from the exit plane until the steady jet region is reached, when it becomes constant. The unsteadiness of the synthetic jet is caused by the high frequency cyclic change of suction

and blowing. The continuous increase in peak local velocity phase within the unsteady jet region is attributed to a momentum transfer time delay within the jet. The constant peak velocity phase in the steady jet region shows that the effect of the SJG suction stroke is confined to the unsteady jet region and only the blowing stroke effects the steady jet region resulting in a steady jet.

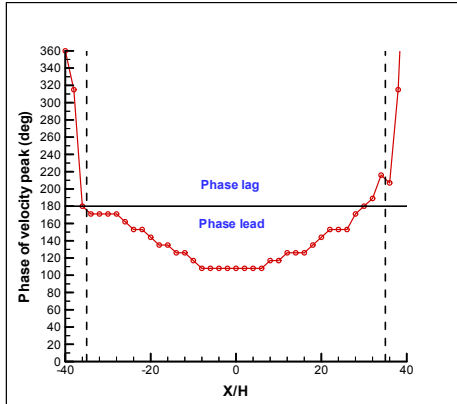


Fig. 17. Variation of peak local velocity phase with longitudinal distance from the slot centre (X/H)

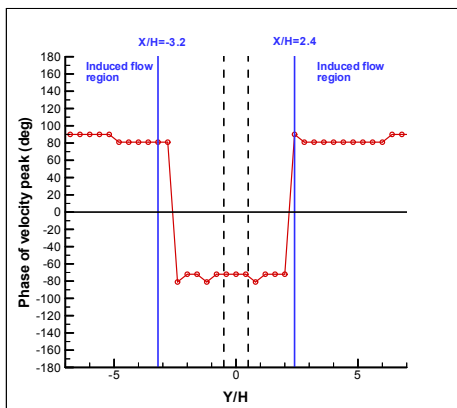


Fig. 18. Variation of peak local velocity phase with lateral distance from the slot centre (Y/H)

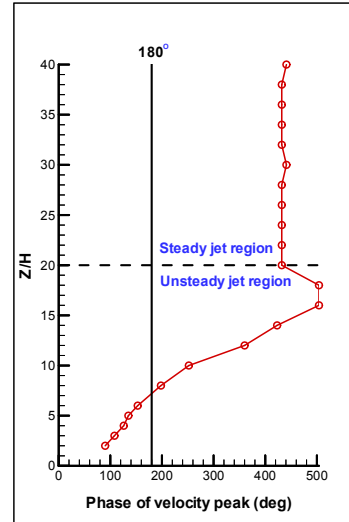
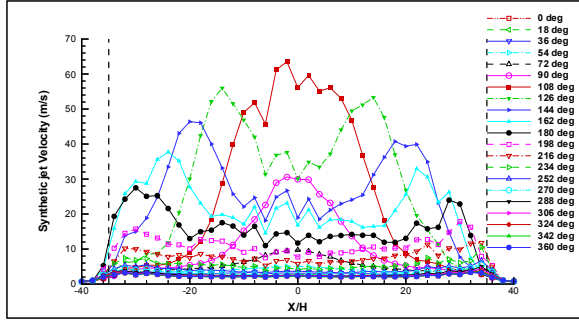


Fig. 19. Variation of peak local velocity phase with vertical distance from the jet exit plane (Z/H)

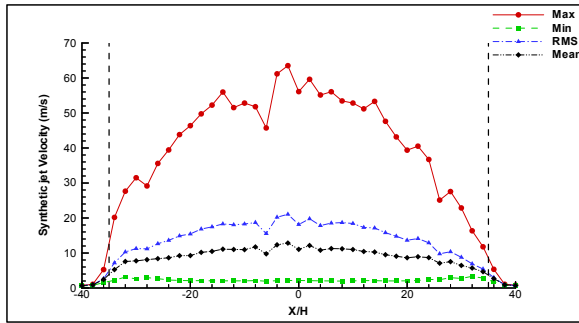
4.5 Velocity profile analysis.

Figures 20, 21 and 22 present the instantaneous velocity and time averaged velocity profiles, for a single operation cycle of the SJG, along each axis of the jet orifice. As can be seen in Figure 20, while the time averaged longitudinal velocity profiles appear parabolic, the instantaneous velocity profiles show that there are significant changes with phase angle throughout the SJG cycle - the profile begins with a ‘bell’ shape and is transformed to ‘saddle’ shape. This profile change is caused by the sequential momentum transfer delay which is shown in Figures 14 and 17.

The instantaneous transverse velocity profiles give information relating to the vortex pair formation around the slot. Since the instantaneous velocity profiles are symmetric about $Y/H=0$, the vortex ring structure is also assumed to be symmetric, see Figure 21. It is clear that the fluctuation in velocity within the jet is reduced with increasing distance (Z/H) from the slot. This agrees with the assessment shown in Figures 16, 19 and 22 and is related to the boundary between the unsteady and steady jet regions.

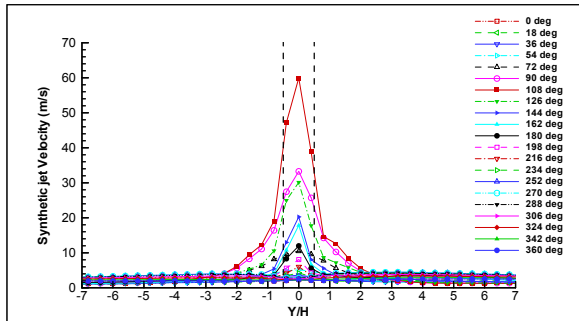


(a) Instantaneous velocity profiles

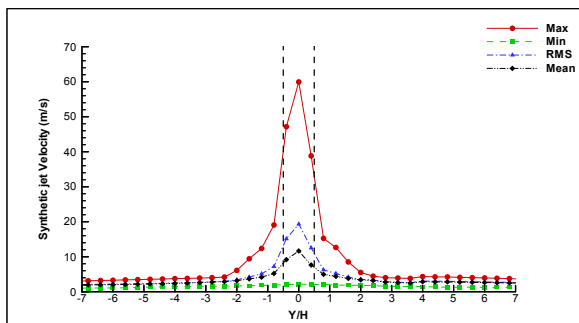


(b) Time averaged velocity profiles

Fig. 20. Longitudinal local velocity profiles ($Y/H=0$, $Z/H=3$)

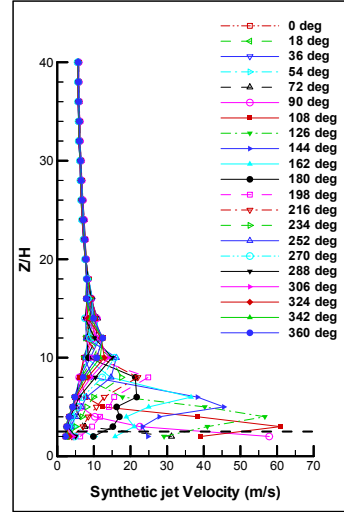


(a) Instantaneous velocity profiles

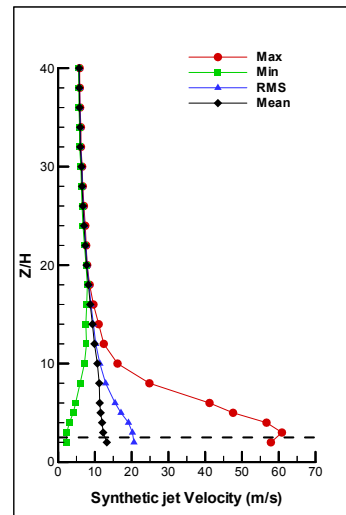


(b) Time averaged velocity profiles

Fig. 21. Lateral local velocity profiles ($X/H=0$, $Z/H=3$)



(a) Instantaneous velocity profiles



(b) Time averaged velocity profiles

Fig. 22. Vertical local velocity profiles ($X/H=0$, $Y/H=0$)

4.6 Comparison of NTH and NPS.

The variation of normalized time history (NTH) and normalized power spectra (NPS) for local velocity measurements are analyzed for locations along each primary slot axis. NPS data are calculated by breaking a single data-set, sampled at 25kHz for 1 second, into 12 separate sets of 2048 samples, for processing in MATLAB. An ensemble average of the 12 resulting spectra is presented. The NPS are dominated by the SJG fundamental frequency ($F_1=1500\text{Hz}$), as expected, and there is little change with position along the slot (X/H). The formation of induced flow is apparent in the

NTH of Figure 24 and the secondary velocity peaks in Figure 24(b). This induced flow is assumed to be responsible for the second peak (F2) in relative NPS. Further moving of HWA probe shows that the induced flow dominates the flowfield. The fundamental frequency (F1) of Figure 24(c) is driven by induced flow.

5 Conclusions

A Synthetic Jet is formed by cyclic suction and blowing through an orifice, as a result, local flow velocities within the jet are unsteady. A single hot wire anemometer probe is used to investigate the time dependent characteristics of the synthetic jet from a rectangular orifice (with a plan-form aspect of 70), which is created by using a dual piezoelectric diaphragm to excite fluidic resonance of a cylindrical cavity. Analysis of the local flow velocity at different locations in the region of the jet shows significant variations in both magnitude and phase (relative to the excitation of the SJG diaphragm). In particular, velocity profiles, along the longitudinal axis of the slot, exhibit characteristic changes - local velocity maxima migrating from the centre of the slot to the edges during a given cycle. The flow structure across the slot is primarily determined by the externally induced flow which in turn is caused by the suction phase of the synthetic jet cycle. Assessment of the flow structure at increasing distance from the slot exit plane (Z) shows that the synthetic jet changes from an unsteady jet to a steady jet when Z is greater than 20 slot widths.

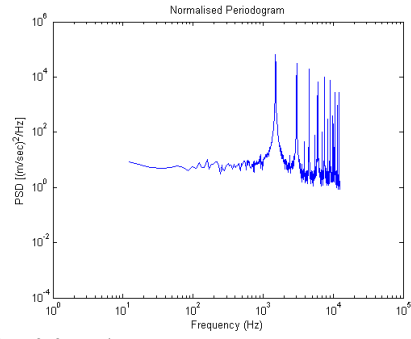
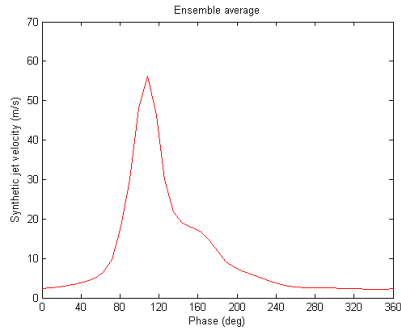
References

- [1] Zhang, X. and Collins, M.W. *Measurement of a Longitudinal Vortex Generated by a Rectangular Jet in a Turbulent Boundary Layer*. Physics of Fluids, Vol.9, No. 6, pp. 1665-1673, 1997
- [2] Bridge, A. and Smith, D.R. *The Influence of Orifice Orientation on the Integration of a Synthetic Jet with a Turbulent Boundary Layer*. AIAA 2001-2774, 2001
- [3] Chambers, F.W. and Jones, G.S. *Density and Mach Number Effects on Piezoelectric Flow Control Actuator Performance*, AIAA 2001-3025, 2001

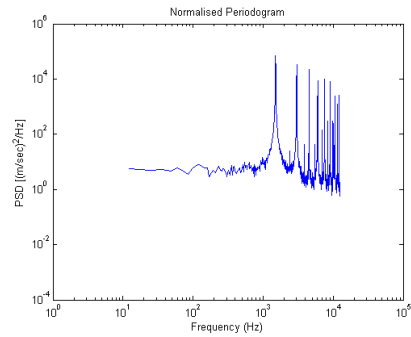
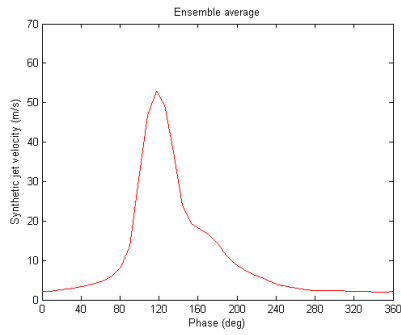
- [4] Utturkar, Y., Mittal, R., Rampunggoon, P. and Cattafesta, L. *Sensitivity of Synthetic Jets to the Design of the Jet Cavity*, AIAA 2002-0124, 2002
- [5] Chungsheng Yao, Fang Jenq Chen, Dan Neuhart, and Jerome Harris, *Synthetic Jet Flow Field Database for CFD Validation*, AIAA 2004-2218, 2004
- [6] Schaeffler, N.W. and Jenkins, L.N. *The Isolated Synthetic Jet in Crossflow: A Benchmark for Flow Control Simulation*, AIAA 2004-2219, 2004
- [7] Lomas, C.G. *Fundamentals of Hot Wire Anemometry*, Cambridge University Press, 1985
- [8] Greitzer, E.M., Tan, C.S. and Graf, M.B. *Internal Flow: Concepts and Applications*, Cambridge University Press, 2007.
- [9] Proakis, J. and Manolakis, D.G. *Digital Signal Processing: Principles, Algorithms, and Applications*, Prentice Hall International Editions
- [10] Murata Manufacturing Company Ltd, "*PZT Application Manual*".

Copyright Statement

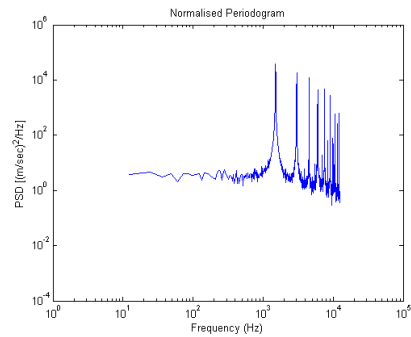
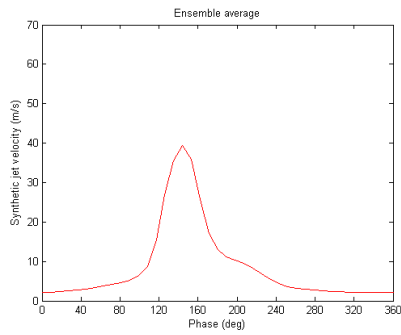
The authors confirm that they, and/or their company or organization, hold copyright on all of the original material included in this paper. The authors also confirm that they have obtained permission, from the copyright holder of any third party material included in this paper, to publish it as part of their paper. The authors confirm that they give permission, or have obtained permission from the copyright holder of this paper, for the publication and distribution of this paper as part of the ICAS2012 proceedings or as individual off-prints from the proceedings.



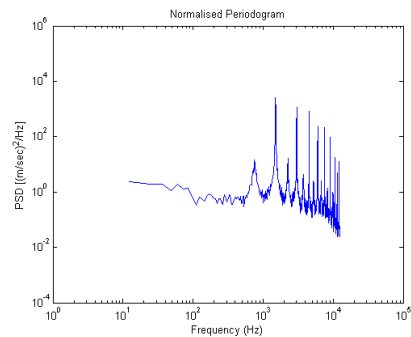
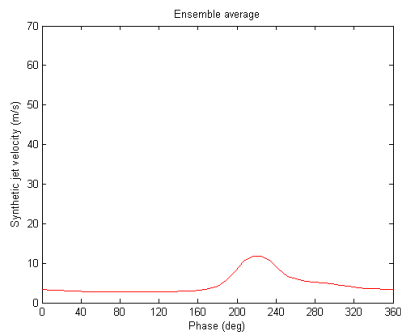
(a) $X/H=0$ ($X=0.0$ mm)



(b) $X/H=10$ ($X=5.0$ mm)



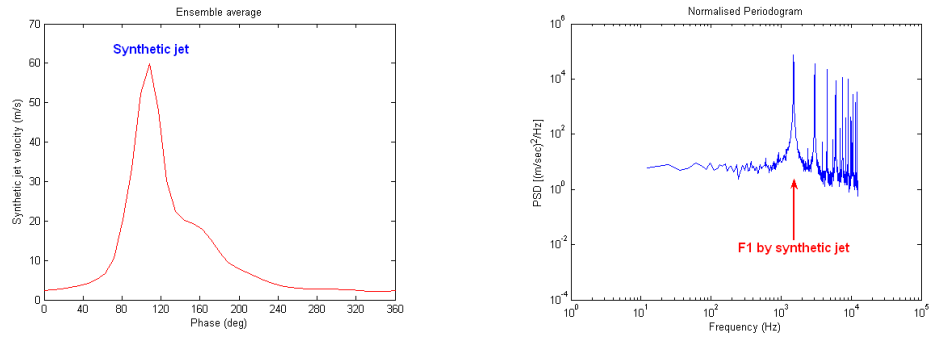
(c) $X/H=20$ ($X=10.0$ mm)



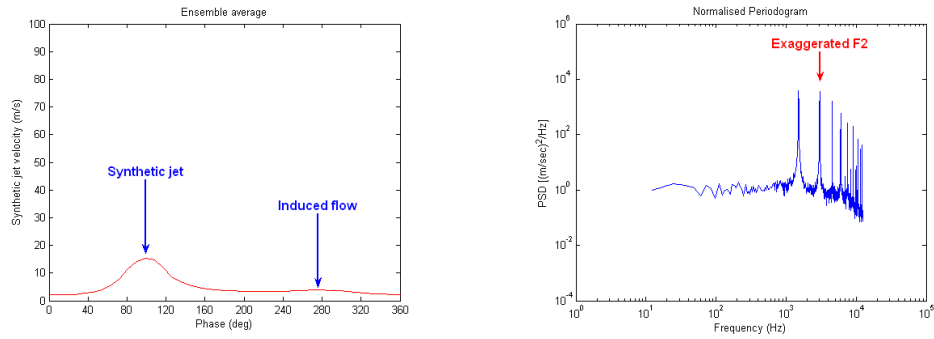
(d) $X/H=34$ ($X=17.0$ mm)

Fig. 23. Variation of local velocity NTH and PSD along the length (X/H) of the jet orifice ($Y/H=0$, $Z/H=3$, $F_s=25$ KHz, $LPF=10$ KHz)

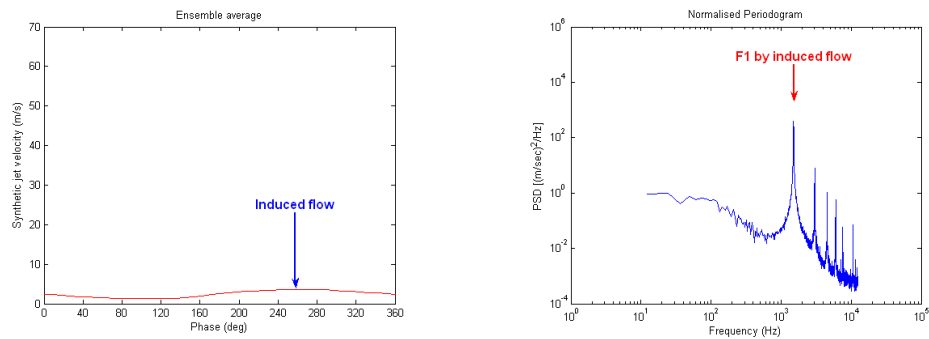
TIME DEPENDENT ANALYSIS OF A RECTANGULAR SYNTHETIC JET



(a) $Y/H=0$ ($Y=0.0$ mm) – synthetic jet region

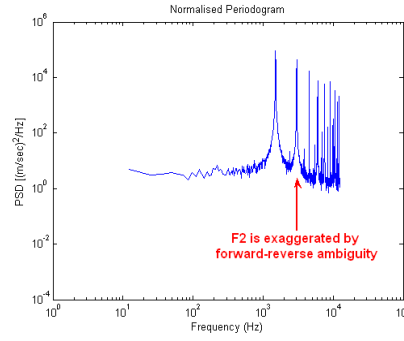
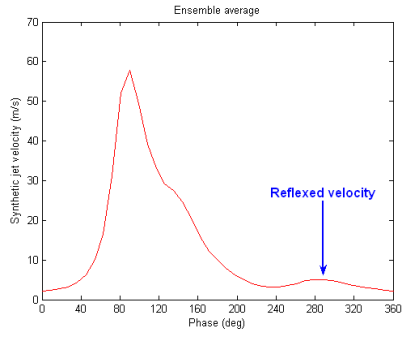


(b) $Y/H=0.8$ ($Y=0.4$ mm) – mixed region

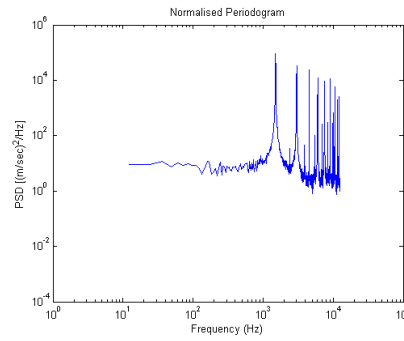
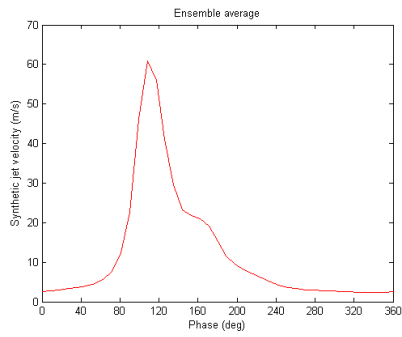


(c) $Y/H=7.2$ ($Y=3.6$ mm) – induced flow region

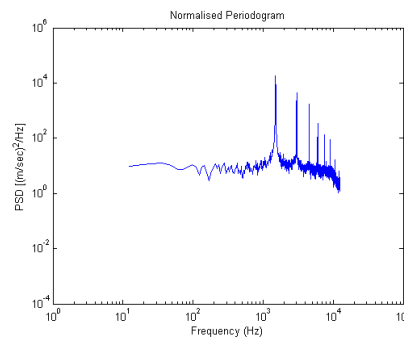
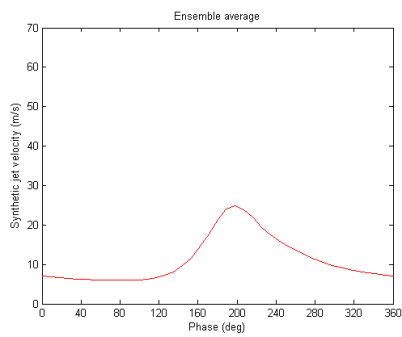
Fig. 24. Variation of local velocity NTH and PSD across width (Y/H) of jet orifice ($X/H=0$, $Z/H=3$, $F_s=25$ KHz, $LPF=10$ KHz)



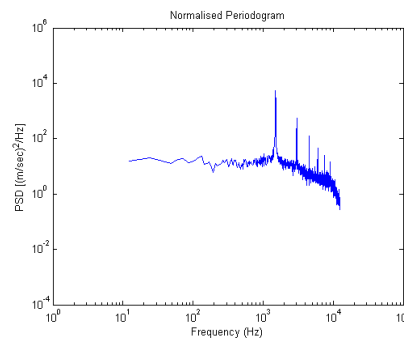
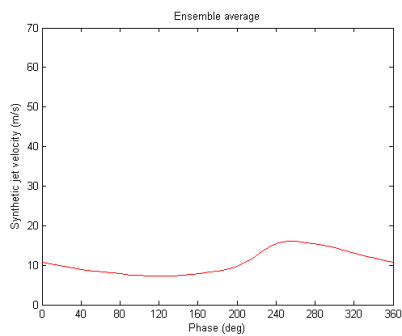
(a) $Z/H=2$ ($Z=1.0$ mm)



(b) $Z/H=3$ ($Z=1.5$ mm)

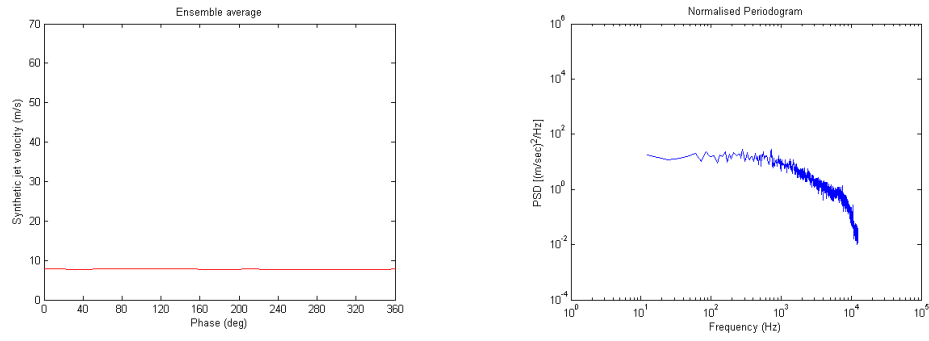


(c) $Z/H=8$ ($Z=4.0$ mm)



(d) $Z/H=10$ ($X=5.0$ mm)

TIME DEPENDENT ANALYSIS OF A RECTANGULAR SYNTHETIC JET



(e) $Z/H=20$ ($Z=10.0$ mm)

Fig. 25. Variation of local velocity NTH and PSD with distance (Z/H) above the jet orifice exit plane ($X/H=0$, $Y/H=0$, $F_s=25$ KHz, $LPF=10$ KHz)